

ARTICLE

Viscous Flow Activation Energy and Short-Term Aging Resistance of SBS-Modified Asphalt Enhanced by PPA Oil-Grinding Activated MoS₂

Shun Chen^{1,2,3}, Yingjie Wang¹, Xingyang He^{1,2,3,*}, Ying Su^{1,2,3}, Yingyuan Pan¹, Yimin Cao¹, Wentian Wang¹, Chao Yang^{1,2,3}, Bo Jiang^{1,2,3} and Shaolin Zhang⁴

¹School of Civil Engineering, Architecture and Environment, Hubei University of Technology, Wuhan, 430068, China

²Building Waterproof Engineering and Technology Research Center of Hubei Province, Hubei University of Technology, Wuhan, 430068, China

³Key Laboratory of Intelligent Health Perception and Ecological Restoration of Rivers and Lakes, Ministry of Education, Hubei University of Technology, Wuhan, 430068, China

⁴China Construction Third Bureau First Engineering Co., Ltd., China

*Corresponding Author: Xingyang He. Email: hexycn@163.com

Received: 04 June 2024 Accepted: 12 October 2024 Published: 06 March 2025

ABSTRACT

Styrene-butadiene-styrene (SBS) modified asphalt (SA) has long found effective applications in road construction materials. When combined with fillers, SBS-modified asphalt has demonstrated promising resistance to fatigue cracking caused by temperature fluctuations and aging. In this study, molybdenum disulfide (MoS₂) and polyphosphoric acid (PPA) were ground in naphthenic oil (NO) and subjected to mechanical activation to create PPA-modified MoS₂, referred to as OMS-PPA. By blending various ratios of OMS-PPA with SBS-modified asphalt, composite-modified asphalts were successfully developed to enhance their overall properties. To assess the mechanical characteristics and stability of these modified asphalts, various methods were employed, including penetration factor, flow activation energy, fluorescence microscopy, and dynamic shear rheology. Additionally, the short-term aging performance was evaluated using Fourier transform infrared (FTIR) spectroscopy and nanoindentation tests. The results revealed a 3.7% decrease in the penetration-temperature coefficient for SA-OMS compared to SA, while 1-SA-OMS-PPA showed an even greater reduction of 7.1%. Furthermore, after short-term aging, carboxyl group generation in SA increased by 5.93%, while SA-OMS exhibited a smaller rise of 1.36%, and 1-SA-OMS-PPA saw an increase of just 0.93%. The study also highlighted significant improvements in the hardness of these materials. The hardness change ratio for SA-OMS decreased by 43.08%, while the ratio for 1-SA-OMS-PPA saw a notable reduction of 65.16% compared to unmodified SA. These findings suggest that OMS-PPA contributed to improvements in temperature sensitivity, particle dispersibility, and resistance to short-term aging in asphalts. The results hold significant promise for the future development of advanced asphalt-based materials with potential high-value applications in flexible pavements for highways.

KEYWORDS

Composite-modified asphalt; grinding; viscous flow activation energy; short-term aging; collaborated



Highlights

- OMS-PPA modified asphalt performed great decreases of penetration-temperature coefficient.
- OMS and OMS-PPA both decreased the viscosity of asphalt at 130°C and 180°C.
- OMS-PPA slightly increased the carboxyl groups of modified asphalt after short-term aging treatment.
- The hardness changes of SA-OMS-PPA decreased greatly after short-term aging process.

List of Abbreviations

SBS	Styrene-butadiene-styrene
SA	Styrene-butadiene-styrene modified asphalt
MoS ₂	Molybdenum disulfide
PPA	Polyphosphoric acid
NO	Naphthenic oil
FTIR	Fourier transform infrared spectrum
SA-OMS	Oil-grinding MoS ₂ modified SA
1-SA-OMS-PPA	PPA-modified MoS ₂ modified SA with 10 g PPA
2-SA-OMS-PPA	PPA-modified MoS ₂ modified SA with 20 g PPA
3-SA-OMS-PPA	PPA-modified MoS ₂ modified SA with 30 g PPA
XRD	X-ray diffraction
SEM	Scanning electron microscope
DSR	Dynamic shear rheometer
TFOT	Thin film oven test
ATR-FTIR	Attenuated total reflection flourier transformed infrared spectroscopy

1 Introduction

Styrene-butadiene-styrene (SBS) modified asphalt (SA) has been widely used as a highway road material. However, rutting and cracking damage under complex conditions can affect the safety of people driving on asphalt roads, especially in overload traffic, friction, and cold and hot alternating environments [1]. Additionally, repairing damaged asphalt pavement requires a significant amount of energy and may result in additional environmental pollution. The new global environmental protection and energy conservation trend is causing researchers to research the use of materials and energies in a clean, low-carbon, and efficient manner. They are gradually implementing various programs to transform and upgrade low-carbon in the road construction and transportation fields. Construction and transportation fields and areas benefit from the extended service life of high-performance asphalt [2]. The life cycle enhancement of asphalt requires both efficient modification approaches and preparation methods [3–5]. Consequently, high-performance modified asphalt has consistently focused on new types of modified asphalt.

Various treatments have resulted in SA performing well against fatigue cracking at low temperatures [6]. Optimizing the mechanical properties and thermal stability of nanomaterials like montmorillonite, tourmaline, and graphene while modifying asphalt is possible [7–10]. The treatment of nano-silica with KH560 can uniformly disperse it in asphalt, enhancing its anti-rutting and high-temperature resistance performance [11]. The performance of aging resistance and storage stability was superior when SA was combined with nano-palygorskite. SA and nano-palygorskite could create an internal homogeneous system that had a spiral-strengthening structure [12]. SA doped with various nano-Al₂O₃ improved its anti-rutting and anti-fatigue properties, storage stability, and aging resistance [13]. SA could benefit from combining with nano-clay and nano-lime to enhance its rheological and anti-rutting performance. The

modifying effect reached its best when SBS, nanoclay, and nano lime were mixed at a moderate level [14]. Two-dimensional nanomaterials, such as MXene nanosheets, could enhance SA's aging resistance performance [15]. The lack of compatibility between nanomaterial and SA could have caused property loss. Surface treatments have been applied to enhance compatibility, but new methods for SA with nanomaterial in an effective manner still pose significant challenges.

Polyphosphoric acid (PPA), a viscous inorganic acid, has the potential to enhance its high-temperature resistance, storage stability, and aging resistance by modifying SA [16]. The high-temperature resistance and thermal stability of PPA-modified asphalt are improved, and its temperature sensitivity is reduced. PPA can achieve chemical reactions and physical mixing effects between asphalt molecules [17,18]. By combining SA with PPA, its hardness may be raised and its anti-rutting, anti-fatigue, and anti-cracking performance may be optimized [19]. SA's deformation resistance and high-temperature stability have been improved by mixing it with PPA and Sasobit [20]. Adding SA to PPA and bio-asphalt could improve its storage stability and protect it against deformation at high temperatures [21]. PPA can enhance the storage stability and rheological properties of crushed rubber-modified asphalt by optimizing crushed rubber [22]. By using PPA, butadiene styrene rubber (SBR) and asphalt can be better compatible and SBR-modified asphalt can have better high and low-temperature properties [23]. However, in-depth work is still needed for the methods and mechanisms of combining modified asphalt with PPA and nanomaterials.

The chemical properties of layered molybdenum disulfide (MoS_2) are distinct and can be utilized in energy, catalysis, and other industries. The layer spacing of MoS_2 is 0.615 nm, which has the potential to be inserted into its crystal between layers due to its weak van der Waals force [24]. The mechanical, anti-aging, and rheological properties of layered nanomaterials modified asphalt have been successfully optimized, including bentonite, layered double hydroxides, graphene, and other materials [25–27]. Viscoelasticity and anti-rutting performances of MoS_2 -modified asphalt were improved by depositing silane and dopamine or co-depositing diethylenetriamine and tannin onto the surface of MoS_2 [28,29]. MoS_2 -modified asphalt could benefit from being combined with fibers to enhance its properties [30]. MoS_2 -modified asphalt could have significant potential advantages due to the layered structure of molybdenum disulfide and the sulfur atoms in MoS_2 . The role of MoS_2 as a modifier of modified asphalt requires further research.

The use of mechanical activation method resulted in the successful preparation of an efficient modifier by grinding MoS_2 in naphthenic oil (NO) with PPA in this study. After preparing SA with a modifier, the performance of composite-modified asphalt was evaluated by analyzing the impact of PPA on it. The study of three indicators and the penetration temperature coefficient of modified asphalt was done to estimate its temperature sensitivity. The storage stability of composite-modified asphalt was calculated by analyzing its viscosity, flow activation energy, and fluorescence microscopy. The viscoelastic and anti-rutting properties of composite-modified asphalt were evaluated using dynamic shear rheology. Development of new road materials that would have high values in high-performance flexible pavement in the future was made possible by the optimization effects of OMS-PPA and SBS on the performance of modified asphalt.

2 Raw Materials and Test Methods

2.1 Raw Materials

The MoS_2 powder (MS, 99.0 wt%) in 1250 mesh was provided by Liaoning Zhonglian Industrial Group Co., Ltd., Liaoning, China. Naphthenic oil (NO) was purchased from Karamay Company, Karamay, China, and linear SBS was purchased from China Petroleum and Chemical Corporation Limited, Beijing, China, as shown in Fig. 1. The matrix asphalt (70#) was supplied by Qilu Petrochemical Company, Zibo, Shandong, China, and the main physical properties are illustrated in Table 1. PPA was obtained from Sigma Aldrich, Shanghai, China, which had a P_2O_5 content exceeding 90%.

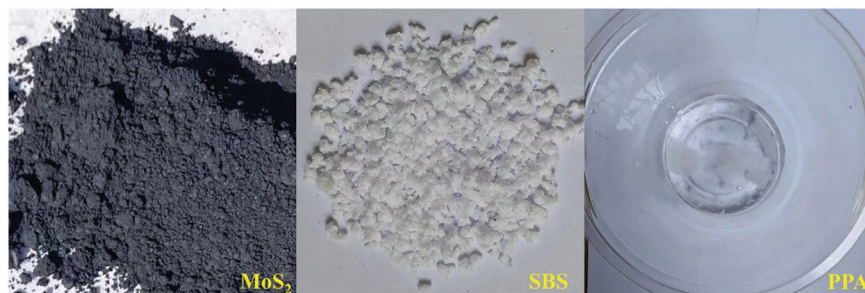


Figure 1: The pictures of MoS₂, SBS and PPA

Table 1: The basic properties of asphalt, MoS₂, SBS, and PPA

Asphalt	Penetration (0.1 mm, 25°C)	Softening point (°C)	Ductility (mm, 10°C)
70#	68.6	47.5	47
MoS ₂	Melting point	Density	Mohs hardness
	1185°C	4.80 g/cm ³	1.5
Linear SBS	Styrene content	Volatile fraction	Total ash
	27.0%	≤1%	≤0.20%
PPA	Melting point	Boiling point	Density
	−20°C	550°C	2.06 g/mL

2.2 Preparation of Modified MoS₂ and Modified Asphalt

After drying at 100°C in an oven for 24 h, 60 g MoS₂ was ground in a planetary ball mill with 150 g NO. Then, 10 g PPA was added to the mixture and mixed. The planetary ball mill was equipped with an appropriate gradation to utilize agate balls (10:8:5 mm) as the grinding medium. After 40 min, the modified MoS₂ was obtained and separated from the slurry, which was then referred to as OMS-PPA. Samples with different weights of PPA (0, 10, 20, and 30 g) were called OMS, 1-OMS-PPA, 2-OMS-PPA, and 3-OMS-PPA, as shown in Table 2. The composite modified asphalt was created by mixing SA (with 5 percent SBS) and 5 wt% OMS, 1-OMS-PPA, 2-OMS-PPA, and 3-OMS-PPA at 170°C and designated SA-OMS, 1-OMS-PPA, 2-OMS-PPA, and 3-OMS-PPA. Both modified asphalts were sheared at a speed of 3000 RPM for 30 min. Then, the asphalt swelled and grew at 130°C for another 30 min. Table 3 shows the various ratios of materials for modified asphalts.

Table 2: Ratios of materials for fabricating OMS-PPA

	MoS ₂	NO	Span 80	PPA
OMS	60 g	150 g	10 g	0 g
1-OMS-PPA	60 g	150 g	10 g	10 g
2-OMS-PPA	60 g	150 g	10 g	20 g
3-OMS-PPA	60 g	150 g	10 g	30 g

Table 3: Materials ratios for preparing SA-OMS-PPA

	Asphalt	SBS	OMS	1-OMS-PPA	2-OMS-PPA	3-OMS-PPA
SA	400 g	20 g	–	–	–	–
SA-OMS	400 g	20 g	20 g	–	–	–
1-SA-OMS-PPA	400 g	20 g	–	20 g	–	–
2-SA-OMS-PPA	400 g	20 g	–	–	20 g	–
3-SA-OMS-PPA	400 g	20 g	–	–	–	20 g

2.3 Test Methods

The chemical groups on the surfaces of NO, MS, OMS, and OMS-PPA were analyzed using a Fourier transform infrared spectra (FTIR) spectrometer (Thermo Fisher Nicolet IS50, USA) from 400 to 4000 cm^{-1} at room temperature. The X-ray diffraction (XRD) patterns of MS, OMS, and OMS-PPA were recorded by a high-resolution powder X-ray diffractometer (Empyrean, Almelo, Netherlands) with a copper target. The morphology of MS, OMS, and OMS-PPA was investigated on a scanning electron microscope (SEM, JEOL JSM6390LV, Tokyo, Japan) with an acceleration voltage range from 0.1 to 30 kV. The basic properties of SA, SA-OMS, and SA-OMS-PPA were analyzed based on the standards (ASTM D36, ASTM D113, and ASTM D5), which included its penetration, softening point, and ductility. A rotational viscometer (Brookfield, Massachusetts, USA) was used to test the viscosity values of SA, SA-OMS, and SA-OMS-PPA at temperatures between 130°C to 180°C with a 10°C span. A dynamic shear rheometer (DSR, Anton Paar Smartpave102, Austria) was utilized to test the rheological behavior of SA, SA-OMS, and SA-OMS-PPA. DSR values were maintained by operating at a fixed frequency of 10 $\text{rad}\cdot\text{s}^{-1}$ at 45°C to 90°C per 5°C. A fluorescence microscope (Leica M205FA, Germany) was used to observe the particle dispersion of SA, SA-OMS, and SA-OMS-PPA. The thin film oven test (TFOT) was used in this experiment to evaluate the short-term aging behavior of SA, SA-OMS, and SA-OMS-PPA in compliance with ASTM-D1754 standards. The SA, SA-OMS, and SA-OMS-PPA were subjected to heating at 163°C for 5 h during this artificial simulation aging procedure. The spectral method used to evaluate the carbonyl index of SA, SA-OMS, and SA-OMS-PPA involved the use of an attracted total refraction model (ATR-FTIR) on a Thermo Fisher Nicolet IS50, which is from the USA. The surficial micromechanical properties of SA, SA-OMS, and SA-OMS-PPA were tested using a nanoindentation instrument (NANOVEA CB500, USA) with a maximum load of 0.12 mN.

3 Results and Discussion

3.1 Properties of OMS-PPA

The FTIR spectra of NO, MS, OMS, and OMS-PPA were shown in Fig. 2. Approximately 480 cm^{-1} was observed with identical peaks due to the stretching vibration of the Mo-S bond from the spectra of MS, OMS, and OMS-PPA [31]. The OMS spectra showed peaks at 2923 and 2852 cm^{-1} that were much more clearly, along with 1456 and 1375 cm^{-1} . The surface or interlayer of MS had NO adsorbing causing these peaks. OMS was activated by the milling balls while grinding the rotating planetary mill. The stretching vibration of P-O is found in the molecule structure of PPA and is represented by new peaks at 1131 and 985 cm^{-1} when compared to OMS. The stretching vibration of O-H can be identified by the peak at 3500 cm^{-1} . The evidence showed that PPA grafted and created many hydrogen bonds between OMS.

The (002) plane of MS was reflected in both peaks on $2\theta = 14.44^\circ$ in the XRD patterns of MS, OMS, and OMS-PPA shown in Fig. 3. The interlayer distances of MS were estimated using Bragg's equation. Both the interlayer spaces of MS, OMS, and OMS-PPA were 0.613 nm, as determined by the formula. XRD patterns

did not influence the differences between MS, OMS, and OMS-PPA. MS has adapted a layered crystalline structure that consists of a Mo atomic layer sandwiched between S atomic layers by bonds [24]. MS, OMS, and OMS-PPA's XRD intensity values changed from decreasing to increasing during the first peak. The contour of the OMS-PPA in Fig. 4 was characterized by a peeled layered structure, which was more noticeable than MS and OMS. Partial loading of NO molecules caused contrast changes in the SEM image of OMS-PPA. Under the influence of mechanical force, a large number of active sites on OMS-PPA could be generated.

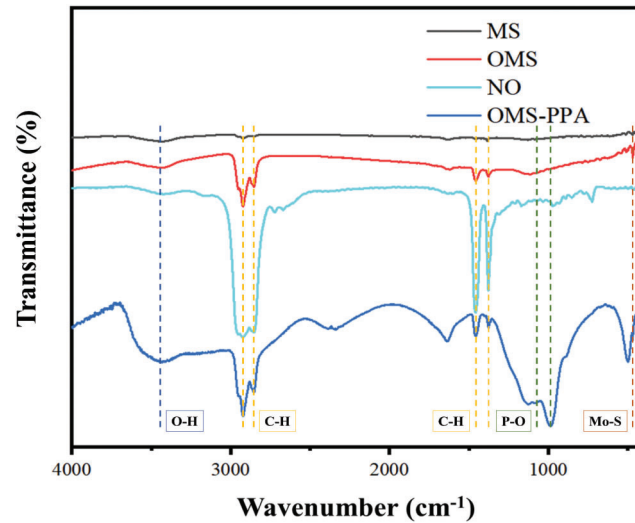


Figure 2: The FTIR spectra of MS, OMS, NO, and OMS-PPA

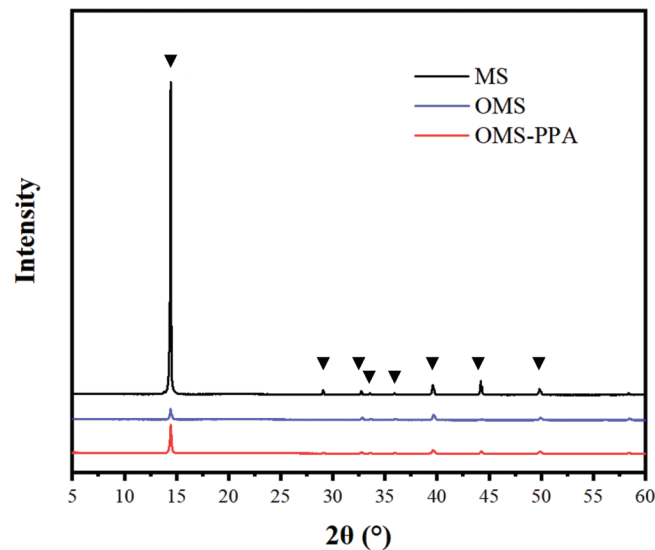


Figure 3: The XRD of MS, OMS, and OMS-PPA

3.2 Physical Properties of Asphalts

To estimate their basic properties, Fig. 5 shows the testing of SA, SA-OMS, and SA-OMS-PPA's ductility, softening point, and penetration. SA-OMS and 1-SA-OMS-PPA had a 111.6% and 30.2%

increase in ductility when compared to SA. OMS enhanced the asphalt’s ability to resist displacement. The interaction between asphalt molecules and OMS particles was increased by PPA, which resulted in a reduction in resistance effects between them. As the amount of PPA used in OMS-PPA increased, the ductility of modified asphalt decreased sharply. The basic requirements of modified asphalt were not met by 2-SA-OMS-PPA and 3-SA-OMS-PPA, even though the added OMS-PPA was 5 wt%. The surface of MS was activated by NO, causing SA-OMS-PPA to have a lower softening point than SA. The dispersibility of OMS particles in asphalt was superior to that of common layered materials. When compared to SA, 1-SA-OMS-PPA had a softening point that was 1.1% higher. The interaction between asphalt molecules and particles led to a higher softening point of SA-OMS-PPA compared to SA after being modified by OMS and PPA. A growing trend was observed in the softening points of 1-SA-OMS-PPA, 2-SA-OMS-PPA, and 3-SA-OMS-PPA when the amount of PPA grew. Additionally, the penetration of 1-SA-OMS-PPA exceeded SA by 61.3%. The potential reaction between PPA and asphalt resulted in a boost in 1-SA-OMS-PPA’s ductility and softening point.

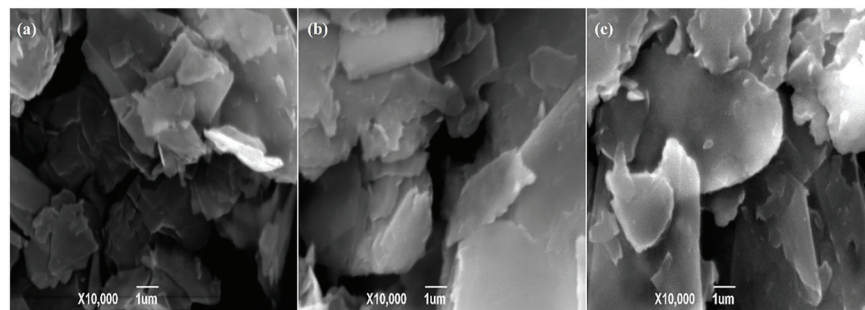


Figure 4: The SEM images of (a) MS, (b) OMS and (c) OMS-PPA

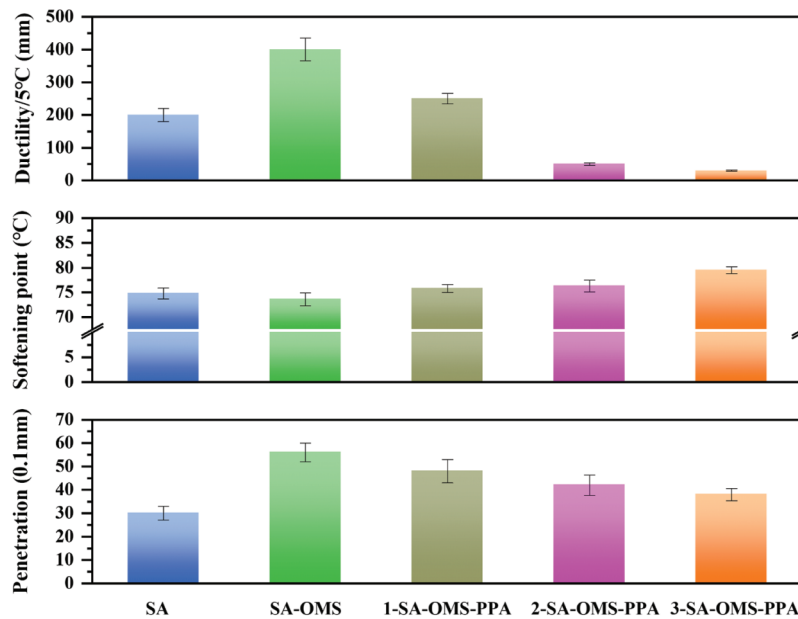


Figure 5: The ductility, softening point, and penetration of SA, SA-OMS, 1-SA-OMS-PPA, 2-SA-OMS-PPA and 3-SA-OMS-PPA

The temperature sensitivity and colloidal structure of modified asphalts can be characterized by the penetration temperature coefficient and penetration factor [32]. Linear fitting was used to calculate the penetration-temperature coefficients of different modified asphalts with penetration values between 15°C and 30°C, as shown in Fig. 6. As demonstrated in Fig. 7, the penetration factors of various modified asphalts can be further calculated. In Fig. 6, the penetration-temperature coefficient of SA-OMS decreased by 3.7% compared to SA. The dispersion of OMS particles was optimized by OMS's surface being able to bring in a small number of lightweight components. The modified asphalt and the integrity of the asphalt system became stronger thanks to the enhanced role of OMS. Compared to SA, 1-OMS-PPA, 2-OMS-PPA, and 3-OMS-PPA experienced a decrease of 7.1%, 9.5%, and 11.2% in their penetration temperature coefficient. The penetration temperature coefficients of modified asphalts decreased as PPA levels increased. The stability of modified asphalts could be improved by PPA's interaction with the asphalt molecules. The temperature sensitivity of modified asphalt is significantly reduced by PPA's effects [33]. According to Fig. 7, the increase in penetration factors was correlated with the decrease in penetration-temperature coefficient. The temperature sensitivity of modified asphalt was reduced by the OMS and PPA due to its penetration factors. The combination of Figs. 6 and 7 resulted in OMS-PPA's critical role in optimizing the stability of modified asphalt, and it could strengthen the gel structure of modified asphalt. The findings showed that PPA molecules had a substantial effect on the consolidation of modified asphalt.

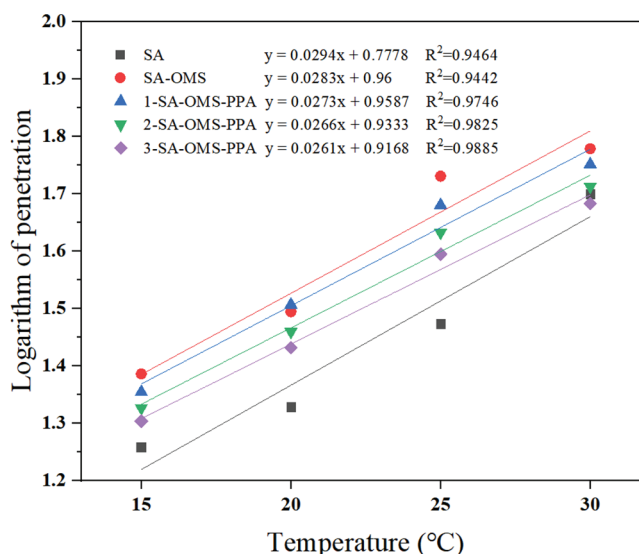


Figure 6: The penetration-temperature coefficient of SA, SA-OMS and SA-OMS-PPA

In Fig. 8, the modified asphalts showed good dispersion under fluorescence irradiation, as evidenced by fluorescence microscopy images. The luminescent groups present in SBS molecules allow for the observation of bright light spots of modified asphalt during fluorescence microscopy images [34]. The fact that SBS dispersed evenly at a combined treatment temperature of 170°C in SA is indicative of its good dispersion at lower stirring temperatures, as seen in Fig. 8a. The uniformity of the dispersed spots of the modified asphalt was achieved when OMS mixed with SA under similar conditions. In SA-OMS, OMS and SBS could interact, which improved the dispersion and compatibility of SBS in SA-OMS in Fig. 8b. The distribution of OMS was difficult to observe due to its weak fluorescence. As demonstrated in Fig. 8c–e, there was an increase in the dispersion of spots in the SA-OMS-PPA. The distribution of SBS modified asphalt by 1-SA-OMS-PPA was superior to that of SA-OMS. Following PPA's adjustments,

OMS grafted additional functional groups, which could potentially interact with the asphalt molecules in 1-SA-OMS-PPA. The clustering of spots is observed in Fig. 8d,e. The mixing ratios of materials during experiments resulted in a gradual increase in PPA compared to 1-SA-OMS-PPA, 2-SA-OMS-PPA, and 3-SA-OMS-PPA. PPA molecules had a significant potential reactivity with asphalt molecules [35]. When combined with Figs. 6–8, the results showed that OMS-PPA had a significant strengthening effect on optimizing the modified asphalt.

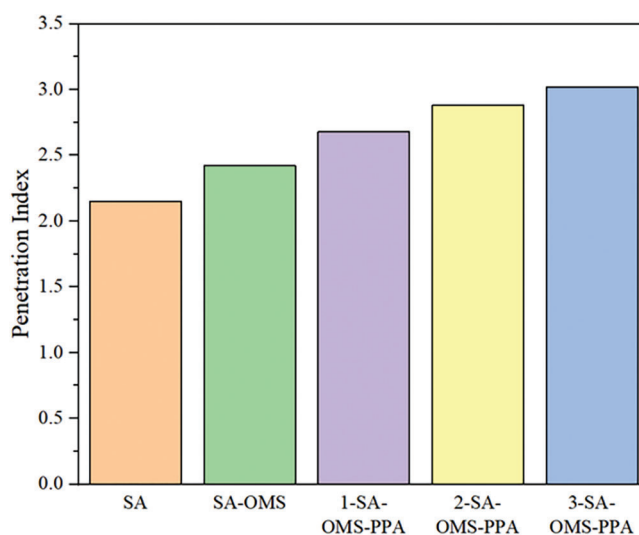


Figure 7: The penetration index of SA, SA-OMS and SA-OMS-PPA

3.3 Viscosity of Asphalts

By analyzing the melting processing of asphalt in Fig. 9, it tested the viscosity of modified asphalt with a fixed torque and shear rate. The viscosity of SA at 130°C was 11.08 Pa·s, as shown in Fig. 9. SA-OMS had a viscosity decrease of 47.65% compared to SA. By facilitating the use of lightweight components, it improved the flow of molecules in modified asphalt [36]. Ultimately, it decreased the viscosity values of asphalt in the Newtonian region. At 130°C, SA-OMS showed a 23.47% decrease in viscosity, while 1-SA-OMS-PPA experienced a 46.2% increase. SA-OMS-PPA had a 13.33% increase in viscosity at 180°C, while the viscosity at SA-OMS-PPA decreased by 34.78% more than SA-OMS. The viscosity of SA-OMS-PPA increased in comparison to 1-SA-OMS-PPA, 2-SA-OMS-PPA, and 3-SA-OMS-PPA. More potential cross-linking points were created with the asphalt molecules in SA-OMS-PPA due to the interaction between PPA molecules on the OMS surface and the asphalt molecules in SA-OMS-PPA. Thermal shearing can lead to the disintegration and reconstruction of this approximate spatial network structure, while the viscosity of modified asphalt continues to increase. The modified asphalt with higher PPA content had more cross-linking points, which led to a higher shearing viscosity value of SA-OMS-PPA. In Fig. 10, the thermal stability of SA-OMS-PPA can be examined by combining the rheological properties of asphalt at different temperatures and the Arrhenius equation. Linear fitting of viscosity values can be used to estimate the activation energy of modified asphalts between 130°C and 180°C. The fitted lines had R^2 values that were more significant than 0.98, indicating a higher degree of fitting reliability. To overcome obstacles caused by internal cross-linking, modified asphalt requires the force represented by activation energy. The difficulty of flowing molten asphalt and its sensitivity to temperature are visually illustrated. It was revealed that PPA could increase the temperature sensitivity of asphalt. Excessive PPA could cause the asphalt system to be unstable and decrease its reinforcing effect

on the asphalt. PPA is likely to react with water molecules in the air and cause side reactions in asphalt systems due to its potential reactivity.

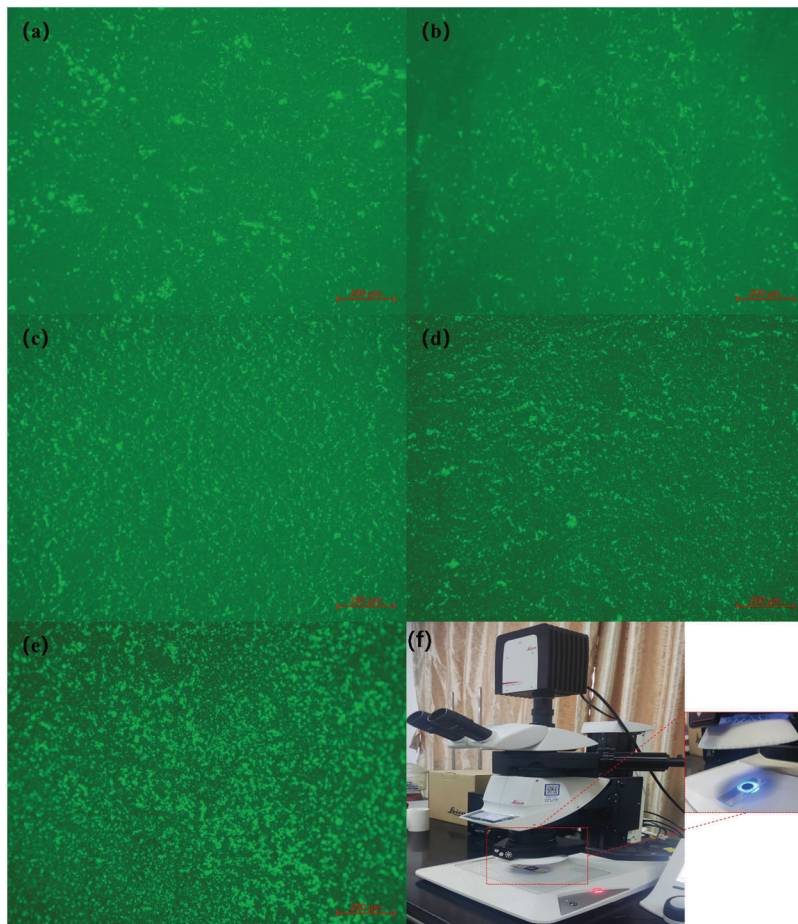


Figure 8: The fluorescence microscope images of (a) SA, (b) SA-OMS, (c) 1-SA-OMS-PPA, (d) 2-SA-OMS-PPA, (e) 3-SA-OMS-PPA and (f) fluorescence microscope and sample

3.4 DSR of Asphalts

Fig. 11 was used to analyze the rheological properties of modified asphalt at different temperatures, using the principle of time-temperature equivalence. As shown in Fig. 11a, SA-OMS's storage modulus (G') at 45°C reduced by 41.52% compared to SA. The storage modulus value of 1-SA-OMS-PPA was higher by 21.49% compared to SA-OMS. The activation of NO molecules on the surface of MoS_2 resulted in asphalt molecules being prone to movement between them. The elastic behavior of 1-SA-OMS-PPA was enhanced by many groups of PPA's potential interactions with asphalt molecules after further modification by PPA. The increase in PPA caused a sharp increase in the elastic modulus of modified asphalt [21]. The internal interaction and elastic behavior of modified asphalts were enhanced due to its improvement. Asphalt lost its elastic behavior as the temperature rose, turning it from viscoelastic to flowing liquid. SA-OMS' loss modulus (G'') decreased by 45.266% at 45°C when compared to SA, while 1-SA-OMS-PPA's storage modulus increased by 13.18% more than SA-OMS, as seen in Fig. 11b. The elastic modulus and the loss modulus had similar trends. The elastic behavior of asphalt could be optimized by combining both

asphalts modified with OMS and OMS-PPA with Fig. 11a,b. The storage modulus value of 1-SA-OMS-PPA was 17.56% higher than SA-OMS, while the $\tan\delta$ at 45°C of SA-OMS decreased by 43.4% more compared to SA. Modified asphalts' $\tan\delta$ exhibited an increasing trend as the temperature increased, but the degree was not the same. The molecular motion of the modified asphalt increased in activity as temperature increased, leading to a gradual transition into a fluid state. SA-OMS had a decrease in elastic properties, while modified asphalt had an increase in viscous properties. Despite the decrease in viscous properties of modified asphalt, the elastic properties of 1-SA-OMS-PPA increased more than SA-OMS. As demonstrated in Fig. 11d, the temperature had a negative impact on the rutting factors ($G^*/\sin\delta$) of modified asphalts. The $G^*/\sin\delta$ at 45°C of SA-OMS and 1-SA-OMS-PPA were both less than SA, but the $G^*/\sin\delta$ of 1-SA-OMS-PPA was more significant than that of SA-OMS. Modified asphalts experienced a significant increase in $G^*/\sin\delta$ as the amount of PPA increased. OMS-PPA was found to have a significant impact on the viscoelastic behavior of modified asphalts.

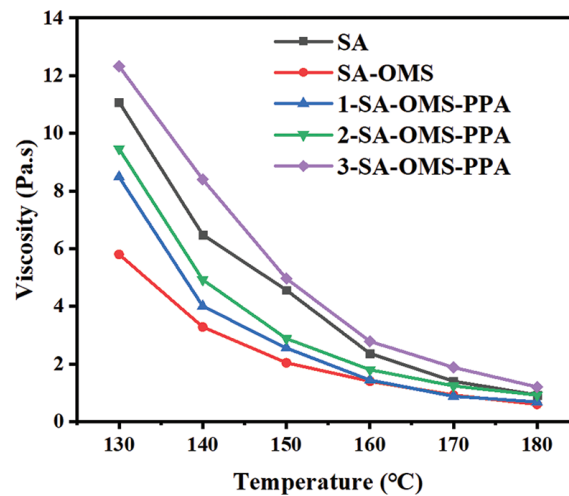


Figure 9: The viscosity values of SA, SA-OMS and SA-OMS-PPA

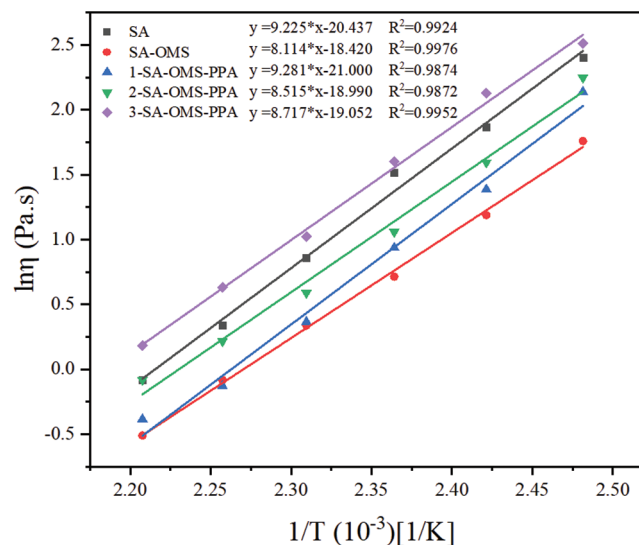


Figure 10: The viscous flow activation energy of SA, SA-OMS and SA-OMS-PPA

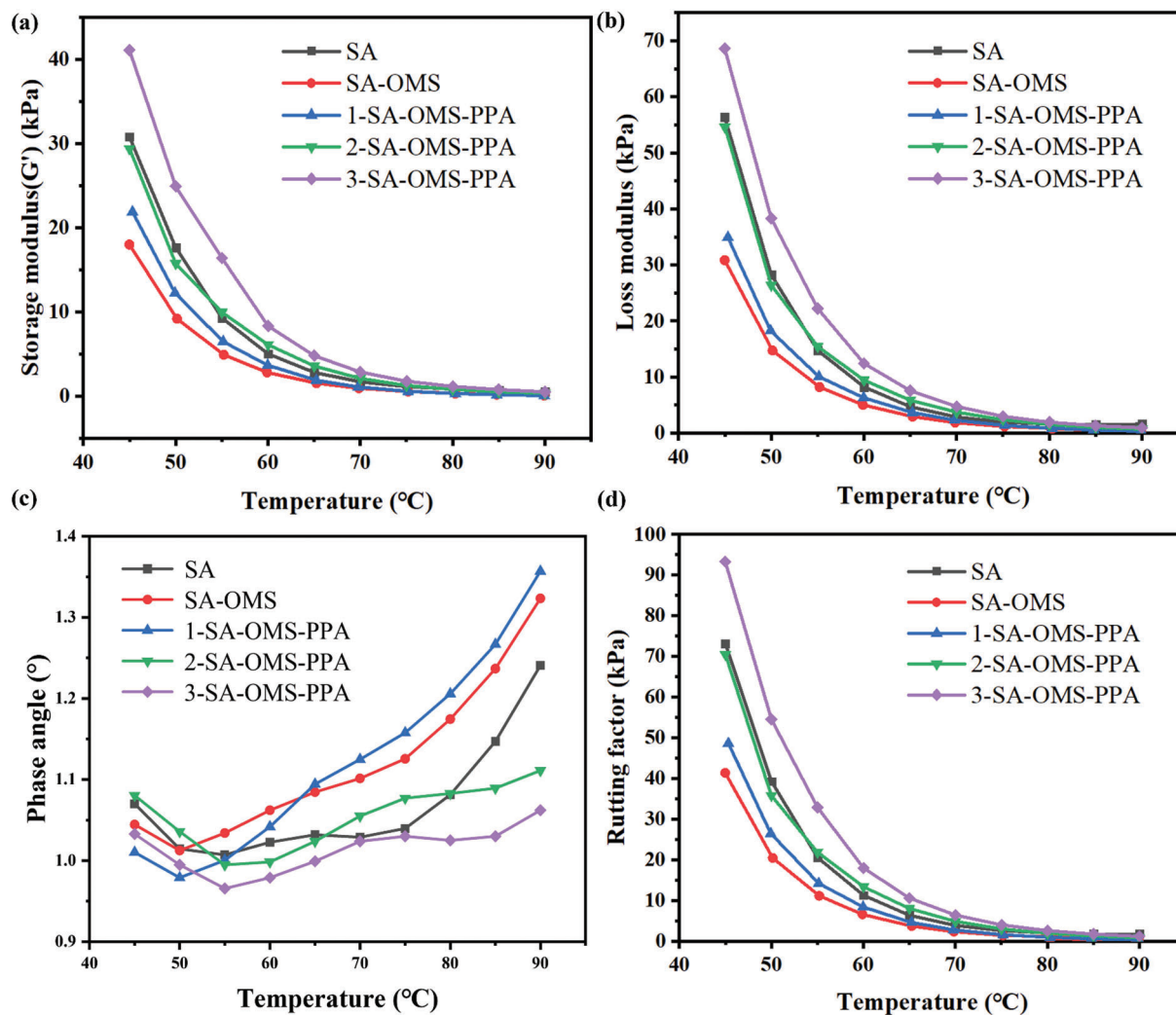


Figure 11: The (a) storage modulus, (b) loss modulus, (c) phase angle and (d) rutting factor ($G''/\sin\delta$) of SA, SA-OMS and SA-OMS-PPA

The main substance of asphalt was hydrocarbons, which would form new carbonyl groups when the molecule chain breaks down during irradiation or oxidation conditions [37,38]. In Fig. 12, the functional group changes of modified asphalt were analyzed using ATR-FTIR. Absorption peaks were found in the unaged modified asphalt at 2960 and 2870 cm^{-1} , which are associated with the $-\text{CH}_2$ groups, and a peak at 1380 cm^{-1} , which is associated with the $-\text{C}-\text{CH}_3$ groups. Carbonyl peaks did not occur on the curves of unaged asphalts, including SA, SA-OMS, and SA-OMS-PPA, when modified asphalts were unaged. A carbonyl peak of 1699 cm^{-1} was observed in modified asphalts after the RTFO test. The peaks at 1699 cm^{-1} were quite distinct from those of SA, SA-OMS, and 1-SA-OMS-PPA. By comparing the curves in Fig. 13, it is possible to estimate the percentage of carbonyl groups in aged asphalts. Short-term aging resulted in a 5.93% increase in the carboxyl groups ($\text{C}=\text{O}$, 1699 cm^{-1}) generated in SA. SA-OMS and 1-SA-OMS-PPA experienced a 1.36% and 0.93% increase in their carboxyl groups, respectively. The amount of carboxyl groups in 2-SA-OMS-PPA was 1.45%, while that of 3-SA-OMS-PPA was 1.52%. Both OMS and OMS-PPA were shown to be capable of delaying the aging of modified asphalt. The effects of 1-SA-OMS-PPA were superior compared to other modified asphalts. The oil grinding process

resulted in a reduction in MS particle size and an increase in its specific surface area. Certain aromatic compounds and polymers can be absorbed from asphalt using this method. Additionally, NO is capable of compensating for the volatilization and oxidation of light components in asphalt during the aging process. The dosage of PPA led to a gradual decrease in the aging resistance performance of modified asphalts, but an increase in the dosage of OMS.

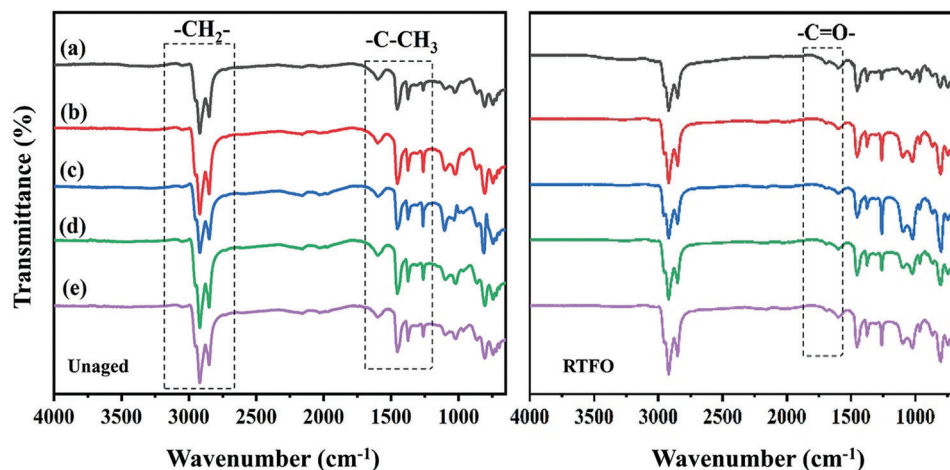


Figure 12: The FTIR curves of (a) SA, (b) SA-OMS, (c) 1-SA-OMS-PPA, (d) 2-SA-OMS-PPA, and (e) 3-SA-OMS-PPA under Unaged and RTFO

By pressing an indenter into the sample shown in Fig. 14, it is possible to record the load data and analyze the depth and hardness parameters on the surface of modified asphalts through nanoindentation [39]. Modified asphalt's mechanical properties could be optimized by obtaining the aging degrees and optimization effect after short-term treatment. The maximum depth of modified asphalt will decrease and its hardness will increase as the age degree increases [40]. Different modified asphalts had their maximum depth and hardness distribution listed. The color changed from blue to red, indicating either a gradual increase in hardness value or a gradual decrease in depth. The depth of SA-OMS was higher than SA, while the hardness of SA-OMS was lower. The penetration and $G^*/\sin\delta$ of asphalts were altered in a consistent manner. The asphalt would undergo a transformation from gel structure to sol structure by introducing small molecules of OMS. The depth of 1-SA-OMS-PPA decreased when compared to SA-OMS and 1-SA-OMS-PPA, but it increased in hardness when compared to SA-OMS. The composite system could be transformed into a gel structure by PPA's interaction with asphalt molecules. The RTFO test resulted in a 38.98% decrease in the depth of SA, while the hardness increased by 51.72%. SA-OMS had a depth decrease of 14.28%, but its hardness increased by 29.44%. SA experienced a 15% decrease in depth, but its hardness increased by 18.02%. The depth change ratio of SA was decreased by 63.37% for SA-OMS, and by 61.52% for 1-SA-OMS-PPA. The hardness changing ratio of SA decreased by 43.08%, while 1-SA-OMS-PPA decreased by 65.16%. With the addition of PPA, the aging resistance performance of modified asphalts gradually deteriorated. The instability in its system could be due to the excessive reaction between PPA and asphalt molecules. OMS and OMS-PPA were proven to have aided in optimizing the structure of asphalts and improving their aging resistance performance.

The primary benefit was the enhancement of the dispersibility of MS oil milled by PPA in asphalt and the optimization of temperature sensitivity and aging resistance of modified asphalt. It contributed to the design and preparation of long-lasting asphalt pavements and decreased maintenance costs. Additionally, it may decrease the use of asphalt materials and lessen the impact on the environment.

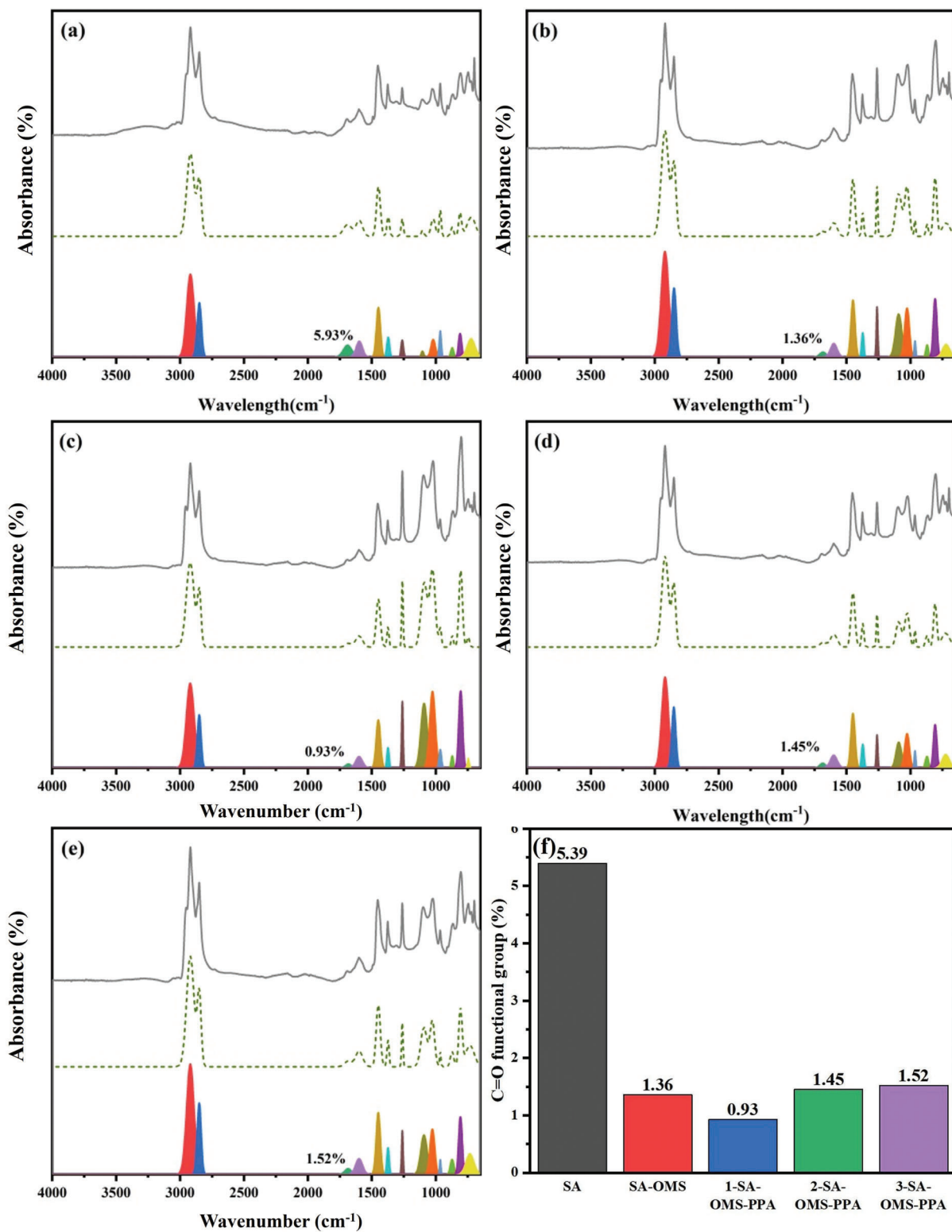


Figure 13: The peaks fitting of (a) SA, (b) SA-OMS, (c) 1-SA-OMS-PPA, (d) 2-SA-OMS-PPA, (e) 3-SA-OMS-PPA, and (f) the percentage of carbonyl groups in asphalts under RTFO

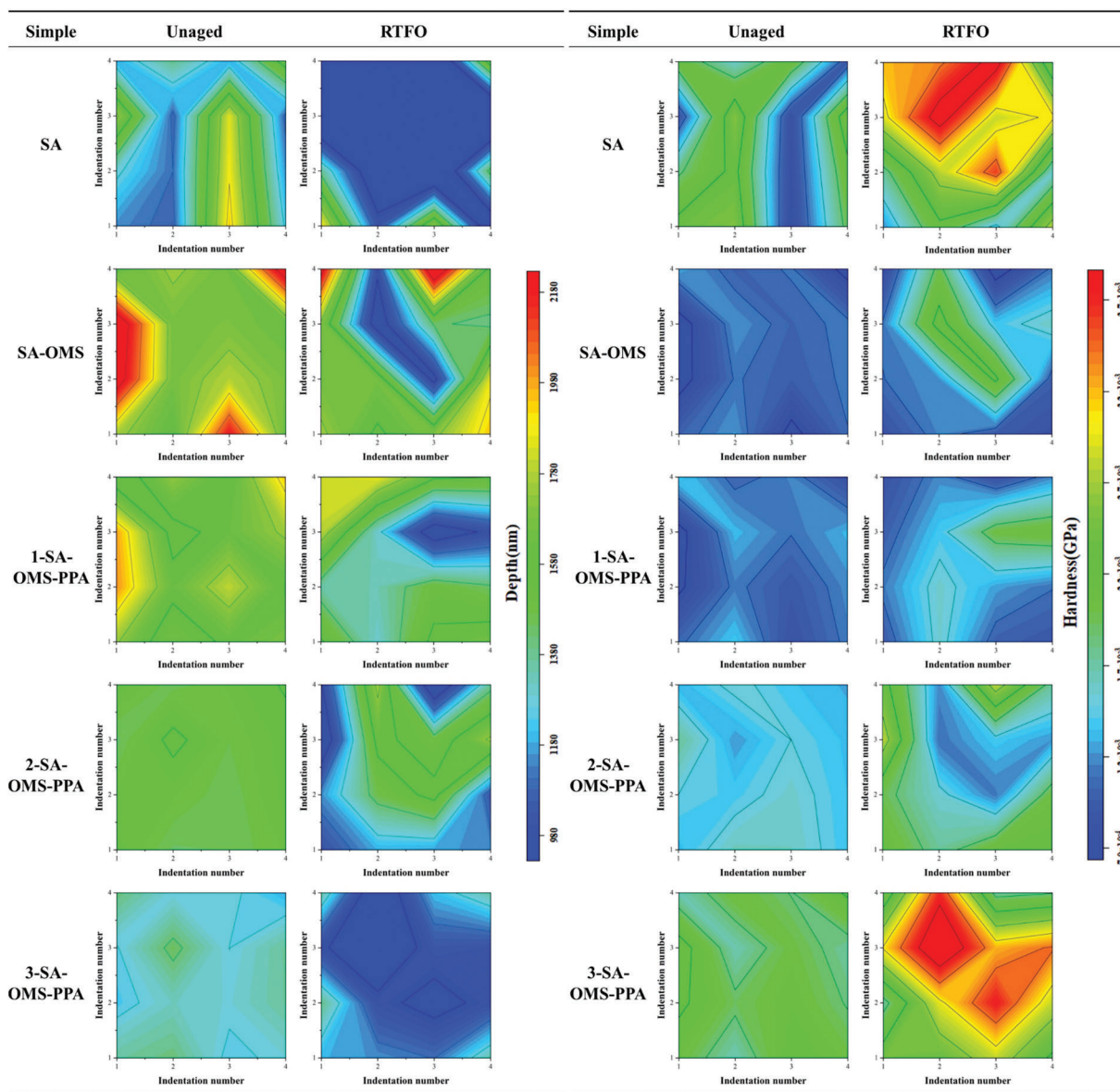


Figure 14: The depth and hardness of SA, SA-OMS, 1-SA-OMS-PPA, 2-SA-OMS-PPA, and 3-SA-OMS-PPA under Unaged and RTFO

4 Conclusions

The fabrication of OMS-PPA was accomplished by grinding MoS₂ and PPA in the NO solvent and preparing modified asphalts by mixing OMS-PPA and SA successfully. The asphalt that had been modified had better mechanical properties and better resistance to short-term aging. It is a highly valuable asphalt material and has great potential for durable pavements in the future. The conclusions are listed as follows:

1. The inner structure of asphalts was optimized by OMS and OMS-PPA, resulting in a reduction in their temperature sensitivity. The penetration temperature coefficient of SA-OMS and 1-SA-OMS-PPA dropped by 3.7% and 7.1% when compared to SA.

2. The activation of asphalt molecules by OMS leads to a decrease in their viscosity. The viscosity of asphalt was increased by PPA reacting with asphalt molecules. SA-OMS-PPA had a 13.33% increase in viscosity at 180°C, while SA-OMS-PPA had a 34.78% decrease in viscosity at 180°C.
3. Short-term aging resulted in lower carboxyl groups generated in SA-OMS-PPA than those generated in SA. The ratios of depth and hardness in SA-OMS-PPA were decreased compared to SA, indicating that OMS-PPA altered the surface structure of asphalt and improved its durability.

Acknowledgement: None.

Funding Statement: The present work is financially supported by the Key Research and Development Program of Hubei Province (Nos. 2022BCA077 and 2022BCA082).

Author Contributions: Shun Chen: Writing original draft, Editing, Supervision. Yingjie Wang: Data processing, Supervision. Xingyang He: Conceptualization, Supervision. Ying Su: Formal analysis, Writing—review. Yingyuan Pan: Methodology, Investigation. Yimin Cao: Data processing, Supervision. Wentian Wang: Data processing, Supervision. Chao Yang: Review, Supervision. Bo Jiang: Review, Supervision. Shaolin Zhang: Review, Supervision. All authors reviewed the results and approved the final version of the manuscript.

Availability of Data and Materials: The data used to support the findings of this study are available from the corresponding author upon request.

Ethics Approval: Not applicable.

Conflicts of Interest: The authors declare no conflicts of interest to report regarding the present study.

References

1. Kumar K, Chand A, Singh RK, Kumar A, Chandra H, Kumar P, et al. Use of modified chitosan as bitumen modifier and its impact on rheological properties in bitumen modification. *Environ Sci Pollut Res Int.* 2024;82(14):1709. doi:10.1007/s11356-024-34860-z.
2. Kappou S, Souliotis M, Papaefthimiou S, Panaras G, Paravantis JA, Michalena E, et al. Cool pavements: state of the art and new technologies. *Sustainability.* 2022;14(9):2022–5159. doi:10.3390/su14095159.
3. Al-Khateeb GG, Alattieh SA, Zeiada W, Castorena C. State-of-the-Art review on the behavior of bio-asphalt binders and mixtures. *Molecules.* 2024;29(16):3835–5. doi:10.3390/molecules29163835.
4. Dalhat MA, Al-Adham K. Review on laboratory preparation processes of polymer modified asphalt binder. *J Traffic Transp Engi (Eng Ed).* 2023;10(2):159–84. doi:10.1016/j.jtte.2023.01.002.
5. Chol BB, Wook PD, Viet VH, Samer D, Sun IJ. Thermal properties of asphalt mixtures modified with conductive fillers. *J Nanomat.* 2015;2015(1):1–6. doi:10.1155/2015/926809.
6. Pandey A, Islam SS, Ransinchung GD, Ravindranath SS. Quantifying the effect of SBS molecular structure on the upper service temperature rheological properties of modified binders. *Constr Build Mater.* 2022;352(9):128826. doi:10.1016/j.conbuildmat.2022.128826.
7. Narayanan SS, Bhupendra S, Ankit K. Chemical treatment of quartzite aggregates and its effect on moisture susceptibility of asphalt mix. *J Mater Civ Eng.* 2024;36(3):04023603. doi:10.1061/JMCEE7.MTENG-17035.
8. Narayanan SS, Ankit K, Bhupendra S. Moisture susceptibility of chemically treated quartzite aggregates in hot mix asphalt. *Int J Pavement Eng.* 2023;24(1):2259575. doi:10.1080/10298436.2023.2259575.
9. Aziz T, Ullah A, Fan H, Jamil MI, Khan FU, Ullah R, et al. Recent progress in silane coupling agent with its emerging applications. *J Polym Environ.* 2021;29(11):3427–43. doi:10.1007/s10924-021-02142-1.
10. Karahancer S. Investigating the performance of cuprous oxide nano particle modified asphalt binder and hot mix asphalt. *Constr Build Mater.* 2019;212(1):698–706. doi:10.1016/j.conbuildmat.2019.04.041.

11. Cai LC, Shi XG, Xue J. Laboratory evaluation of composed modified asphalt binder and mixture containing nano-silica/rock asphalt/SBS. *Constr Build Mater.* 2018;172(2):204–11. doi:10.1016/j.conbuildmat.2018.03.187.
12. Shafabakhsh G, Sadeghnejad M, Daraei I, Sabbaghian H, Ebrahimnia R. The effect of Nano-CaO modified binder on the rutting and fatigue performance of asphalt mixtures. *Case Stud Constr Mater.* 2024;21(1):e03757. doi:10.1016/j.cscm.2024.e03757.
13. Bhat FS, Mir MS. A study investigating the influence of nano Al_2O_3 on the performance of SBS modified asphalt binder. *Constr Build Mater.* 2021;271(1–2):121499. doi:10.1016/j.conbuildmat.2020.121499.
14. Ghanoun SA, Tanzadeh J, Mirsepahi M. Laboratory evaluation of the composition of nano-clay, nano-lime and SBS modifiers on rutting resistance of asphalt binder. *Constr Build Mater.* 2020;238(1):117592. doi:10.1016/j.conbuildmat.2019.117592.
15. Albayati AH, Oukaili NK, Moudhafar MM, Allawi AA, Said AI, Ibrahim TH. Experimental study to investigate the performance-related properties of modified asphalt concrete using nanomaterials Al_2O_3 , SiO_2 , and TiO_2 . *Materials.* 2024;17(17):4279. doi:10.3390/ma17174279.
16. Rani S, Ghabchi R, Ali SA, Zaman M, O'Rear EA. Moisture-induced damage potential of asphalt mixes containing polyphosphoric acid and antistripping agent. *Road Mater Pavement.* 2022;23(12):2818–38. doi:10.1080/14680629.2021.2002180.
17. Ali SA, Foley KA, Zaman M, Walters KB. Microstructural evaluation of the effects of aggregate type, aging, and additives on the moisture susceptibility of binder-aggregate systems using chemical and thermodynamic approaches. *J Mater Civ Eng.* 2024;36(10):04024321. doi:10.1061/JMCEE7.MTENG-17006.
18. Saadeh S, Katawal P, Kabir SF, Fini EH, Titi HH. Performance of reclaimed asphalt pavements containing recycled waste plastics. *J Clean Prod.* 2024;442(1):140935. doi:10.1016/j.jclepro.2024.140935.
19. Liu SJ, Zhou SB, Peng AH. Evaluation of polyphosphoric acid on the performance of polymer modified asphalt binders. *J Appl Polym Sci.* 2020;137(34):48984. doi:10.1002/app.48984.
20. Ge DD, Yan KZ, You LY, Wang ZX. Modification mechanism of asphalt modified with Sasobit and Polyphosphoric acid (PPA). *Constr Build Mater.* 2017;143(3):419–28. doi:10.1016/j.conbuildmat.2017.03.043.
21. Ibrahim H, Alam G, Faheem A. Eco-economic analysis of utilizing high volumes of recycled plastic and rubber waste for green pavements: a comparative life cycle analysis. *Case Stud Constr Mater.* 2024;21(1):e03690. doi:10.1016/j.cscm.2024.e03690.
22. Qian CD, Fan WY, Ren FY, Lv XB, Xing BD. Influence of polyphosphoric acid (PPA) on properties of crumb rubber (CR) modified asphalt. *Constr Build Mater.* 2019;227(1–2):117094. doi:10.1016/j.conbuildmat.2019.117094.
23. Liang P, Liang M, Fan WY, Zhang YZ, Qian CD, Ren SS. Improving thermo-rheological behavior and compatibility of SBR modified asphalt by addition of polyphosphoric acid (PPA). *Constr Build Mater.* 2017;139(1):183–92. doi:10.1016/j.conbuildmat.2017.02.065.
24. Rasamani KD, Alimohammadi F, Sun YG. Interlayer-expanded MoS_2 . *Mater Today.* 2017;20(2):83–91. doi:10.1016/j.mattod.2016.10.004.
25. Chen S, Zhang B, He XY, Su Y, Liu Q, Xu H. Research on mechanical-activated nanoscale bentonite and surface aging behavior of its modified asphalt. *Constr Build Mater.* 2022;321(S1):126356. doi:10.1016/j.conbuildmat.2022.126356.
26. Li YY, Wu SP, Dai Y, Pang L, Liu QT, Nie S, et al. Laboratory and field evaluation of sodium stearate organically modified LDHs effect on the anti-aging performance of asphalt mixtures. *Constr Build Mater.* 2018;189(1):366–74. doi:10.1016/j.conbuildmat.2018.09.021.
27. Li X, Wang YM, Wu YL, Wang HR, Chen M, Sun HD, et al. Properties and modification mechanism of asphalt with graphene as modifier. *Constr Build Mater.* 2021;272(2):121919. doi:10.1016/j.conbuildmat.2020.121919.
28. Pandey A, Islam SS, Ransingchung GD, Ravindranath SS. Comparing the performance of SBS and thermoplastics modified asphalt binders and asphalt mixes. *Road Mater Pavement.* 2023;24(sup1):369–88. doi:10.1080/14680629.2023.2180999.

29. Wang SS, Liu Y, Muhammad Y, Wei YH, Hu CW, Li J. Fabrication of MoS₂-based environment friendly modifier via tannic acid assisted diethylenetriamine co-deposition for the preparation of composite SBS modified asphalt. *Constr Build Mater.* 2021;285(3):122871. doi:10.1016/j.conbuildmat.2021.122871.
30. Zhu ZR, Liu Y, Muhammad Y, Lu WQ, Zhao ZX, Li J. Study on the modified fiber with nacre layer structure based on bionic coating and molybdenum disulfide co-construction incorporated asphalt. *Polym Composite.* 2021;42(10):5374–87. doi:10.1002/pc.26230.
31. Wen X, He C, Hai YY, Liu XF, Ma R, Sun JY, et al. Fabrication of a hybrid ultrafiltration membrane based on MoS₂ modified with dopamine and polyethyleneimine. *RSC Adv.* 2021;11(42):26391. doi:10.1039/d1ra03697a.
32. Lesueur D. The colloidal structure of bitumen: consequences on the rheology and on the mechanisms of bitumen modification. *Adv Colloid Interfac.* 2009;145(1–2):42–82. doi:10.1016/j.cis.2008.08.011.
33. Wei J, Shi S, Zhou Y, Chen Z, Yu F, Peng Z, et al. Research on performance of SBS-PPA and SBR-PPA compound modified asphalts. *Materials.* 2022;15(6):2112. doi:10.3390/ma15062112.
34. Al-Hosainat A, Nazzal MD, Kim SS, Abbas A. Evaluation of field-produced aramid fiber-reinforced asphalt mixtures. *J Mater Civil Eng.* 2024;36(11):04024383. doi:10.1061/JMCEE7.MTENG-17695.
35. Zekel LA, Batov AE, Visaliev MY, Kubrin NA, Dandaev AU, Kadiev KM. Effects of nickel promotion on the catalytic performance of *In Situ* synthesized suspensions of molybdenum disulfide nanoparticles. *Pet Chem.* 2023;63(9):1061. doi:10.1134/S0965544123060300.
36. Kadiev KM, Zekel LA, Kadieva MK, Khadzhiev SN. Formation of polycondensation products in heavy oil feedstock hydroconversion in the presence of ultrafine catalyst: physicochemical study. *Pet Chem.* 2018;58(7):519–27. doi:10.1134/S0965544118070034.
37. Li X, Wang YM, Wu SJ, Wang HR, Liu XC, Sun HD, et al. Effect of montmorillonite modification on resistance to thermal oxidation aging of asphalt binder, *Case Stud Constr Mat.* 2022;16(1391):e00971. doi:10.1016/j.cscm.2022.e00971.
38. Chen S, Pan YY, Zhang B, He XY, Su Y, Liu Q, et al. Preparation and properties of pre-treated nano-bentonite incorporated styrene-butadiene-styrene (SBS) modified asphalt, *Case Stud Constr Mat.* 2023;19:e02505. doi:10.1016/j.cscm.2023.e02505.
39. Uchoa AFJ, Rocha WS, Gonzaga MLC, Filho PPMT, Feitosa JPM, Luna FMT, et al. Investigating the efficacy of bio-rejuvenators in restoring aged asphalt binder properties. *Constr Build Mater.* 2024;446(9):137948. doi:10.1016/j.conbuildmat.2024.137948.
40. Gowda S, Kumar P, Niranjana AS, Gupta A, Kavitha G. Influence of recycled asphalt and rejuvenated recycled asphalt on mechanical performance and chemical makeup of asphalt binder. *IOP Conf Ser: Earth Environ Sci.* 2024;1326(1):012064. doi:10.1088/1755-1315/1326/1/012064.